Regional circulation patterns of Mediterranean Outflow Water near the Iberian and African continental slopes

Álvaro de Pascual-Collar[1,2], Marcos García-Sotillo[1], Bruno Levier[3], Roland Aznar[2], Pablo Lorente[2], Arancha Amo[2], Enrique Fanjul[1]

[1]Puertos del Estado, Avenida del Partenón 10, 28042, Madrid, Spain.
[2]Nologing, Avda. De Ranillas 1D, 50018 Zaragoza, Spain.
[3]Mercator Ocean, 8-10 Rue Hermès, 31520 Ramonville Saint-Agne, France.

Correspondence to: Álvaro de Pascual (alpascua@ucm.es)

Abstract. The Mediterranean Outflow Water (MOW) is a dense water mass originated in the Gibraltar Straight. After exiting the Gulf of Cadiz, the MOW forms a reservoir region west of the Iberian continental slopes with a buoyant depth of approximately 1000m depth. This region is a key role as the main centre where the MOW is mixed and distributed into the North Atlantic. The seafloor in this area is characterised by the presence of a complex bathymetry with three abyssal plains separated by mountain chains. Despite of this topographic features does not reach the surface, they influence ocean flows at intermediate and deep ocean layers conditioning the distribution and circulation of MOW.

The CMEMS IBI ocean reanalysis is used to provide a detailed view of the circulation and mixing processes of MOW near the Iberian and African Continental slopes. This work emphasizes the relevance of the complex bathymetric features defining the circulation processes of MOW in this region. The high resolution of the IBI reanalysis allows to make a description of the meso-scale features forced by the topography. The temperature, salinity, velocity, transport, and vorticity fields are analysed to understand the circulation patterns of MOW. The high-resolution circulation patterns found reveals that Horseshoe Basin and the continental slope near Cape Ghir are key areas controlling the mixing processes of MOW with the surrounding waters mases, mainly North Atlantic Central Water (NACW), and Antarctic Intermediate Water (AAIW). The water masses variability is also analysed by means of composite analysis, results indicate the existence of a variability of the MOW tongue which retracts and expands westwards in opposition to the movement of the underlying North Atlantic Deep Water.

1 Introduction

The Mediterranean Outflow Water (MOW) is a saline and warm water mass principally occupying the intermediate depths of eastern North Atlantic. It is generated from the Mediterranean Sea Water (MSW) outflow occurred through the Strait of Gibraltar. After this subsurface Mediterranean water overpasses the Strait of Gibraltar, the denser MSW cascades along the slope in the Gulf of Cadiz and progressively entrains the ambient North Atlantic Central Water (NACW). On its way down slope, the presence of several transverse submarine valleys leads to splitting up the flow in two different branches with different densities. Although both branches flows separated along different erosive channels, they finally converge near Cape St.

Vincent forming two differenced layers of the same water mass (Iorga and Lozier, 1999a and 1999b, Gasser et al., 2017). Resulting in a buoyant depth around 1000m, MOW exits the Gulf of Cadiz; thereafter it goes northward and enters the Tagus Basin where it turns anticyclonically forming a reservoir of this water mass (Deniault et al., 1994) to the west of Iberian Peninsula. From this reservoir zone, the MOW spreads into the North Atlantic, following two main advective pathways: a

5   westward branch towards the central Atlantic, and a poleward pathway that, driven by the Iberian Poleward Current, follows the western European continental slope. In its way north MOW enters the Bay of Biscay and continues further north towards Porcupine Bank and Rockall Trough, at 53ºN (Reid, 1979, 1994; van Aken and Becker, 1996; Iorga and Lozier, 1999a, 1999b; Bower et al., 2002). On its northward movement the diapycnal mixing with the underlying Labrador Sea Water core (LSW) leads to one of the recognized ways of salt transport into the inner North Atlantic (Talley and McCarney, 1982; van Aken,

10   2000). The influence of MOW flow on the Nordic seas has been discussed in several studies (Reid, 1979, 1994; Bower et al., 2002; Iorga and Lozier, 1999a, 1999b; New et al., 2001; McCarney and Mauritzen, 2001), however later studies suggest that westward shifts of the subpolar front controls the entrance/blocking of Atlantic water through Rockall Trough (Lozier and Stewart, 2008).

Despite of the existence of these two mentioned main pathways, the MOW spreads from the reservoir area by other processes

15   in south and south-western directions, interacting with other surrounding water masses. Thus, another core of MOW spreads south-west largely supported by the motion of Mediterranean Water lenses, so-called meddies (Armi and Zenk, 1984; Armi et al., 1989; Bower et al., 1997; van Aken, 2000). The saline signal of MOW extends southward, reaching Canary Islands where the water mass collides with a diluted form of Antarctic Intermediate Water (AAIW) (Machin et al. 2009; Machín and Pelegí 2010).

20   Several works have focused their attention on the description of MOW in the Gulf of Cadiz, some of them based on observational in-situ data (García-Lafuente et al., 2006; Machín et al., 2009) and some others based in model products (Gasser et al., 2017). The consistency between both approaches has leaded to the knowledge of the oceanographic processes taking place in this area. However, the MOW flowing beyond the Gulf of Cadiz has not been investigated so extensively and the scientific literature is rather limited. Most of the studies on this area are based in compiling data sets of hydrographic stations

25   or climatological data (e.g. Mazé et al., 1997; Iorga and Lozier 1999a; van Aken, 2000). Despite of these methodologies consider a fair number of stations, they usually are affected by a lack of temporal coverage, therefore the results may be affected by seasonal or mesoscale processes. On the other hand, the works that deals with modelling methodologies are usually focused in bigger scales such as the complete eastern North Atlantic (e.g. iorga and Lozier, 1999b; Bozec et al., 2011), and their resolutions are too coarse to provide a proper representation of mesoscale processes in the area. However, several

30   scientific works have described the existence of important mesoscale features in this region such as: the formation of Mediterranean Water lenses (meddies; Armi and Zenk, 1984; Armi et al., 1989; Bower et al., 1997; Deniault et al., 1994; Sangrá et al., 2009), development of an anticyclonic gyre centred in the Tagus Abyssal Plain, and the flow along the Gorringe Bank; highlighting the influence of bathymetry developing mesoscale flows (Zenk and Armi, 1990; Deniault, 1994; Iorga and

Lozier, 1999a, and 1999b). Therefore, we have a good knowledge of the general circulation of MOW, but there is still a lack of knowledge of the circulation patterns affecting this water mass along this region.

Ocean reanalysis provides consistent and realistic 3D gridded ocean fields of the last decades. The combination of numerical ocean model and data assimilation techniques allows to generate a realistic view of the circulation patterns including: (1) high-enough spatial resolution to reconstruct the mesoscale features and (2) long temporal coverage that permits the obtention of averaged fields that show stationary features not affected by temporal variability. The present work uses the Copernicus Marine Environmental Monitoring Service (CMEMS) Iberian-Biscay-Ireland (IBI) reanalysis (Levier et al., 2014, Sotillo et al., 2015, Aznar, 2016, Amo Baladrón, 2018) to make a description of the averaged circulation in the domain defined by the Tagus, Horseshoe and Seine abyssal plains. This work emphasizes the mesoscale features together with the general circulation patterns, and the interannual variability thereof. The CMEMS IBI reanalysis has been produced by the CMEMS IBI Monitoring and Forecasting Centre (IBI-MFC), and it is one of the muti-year data product used in the Copernicus Ocean State Report (von Schuckman et al. 2017, von Schuckman et al., 2018) which is aimed to provide regular and systematic reference information on the physical state, variability and dynamics of the global ocean and European regional seas. In the framework of its second issue, the IBI-MFC proposed an ocean monitoring indicator to characterize the interannual variability of MOW in the IBI region (Pascual et al., 2018); for that purpose an analysis of the circulation patterns, transports and temporal variability of MOW was performed. In the present work, it is summarized part of the results found in the analysis done for the design phase of the CMEMS MOW Ocean Indicator. The resolution of the IBI reanalysis (1/12°, ~8 Km) allowed to observe several circulation features that reveals the important role of bathymetry in the spreading of MOW beyond the Gulf of Cadiz. Additionally, the temporal coverage of the IBI reanalysis (1992-2016) permitted the analysis of the temporal variability resulting in the description of the mid-term variability of MOW in the region.

The paper is organized as follows: a first background of the distribution of MOW near the African and Iberian continental slopes is given in section 2. Description of the IBI reanalysis and the methods used are presented in section 3. Results are presented and discussed in sections 4 and 5: The analysis of flow, transports and hydrographic properties is split in two subsections focused in Tagus and Horseshoe basins (section 4.1) and the African slope near Cape Ghir and Cape Sim (section 4.2); the temporal variability of MOW is studied in section 5. Finally, main conclusions are summarized in section 6.

2 Background on the MOW regional behaviour

The region of study is bounded by the 39°N and 31°N parallels, and by the 15°W meridian and the Iberian and north-west African continental self edges (Figure 1). This domain comprises three abyssal plains oriented from north to south (Tagus, Horseshoe, and Seine) with depths greater than 5000m. These three abyssal plains are separated by a number of seamounts structured in two zonal mountain chains, whose highest peaks are Ampere Bank and Gorringe Bank. The west margin of the plains is limited by the presence of the Azores-Portugal Rise. These promontories are quite high obstacles, exceeding the 500m depth, thereby they define a set of walls around each plain conforming three separated basins.

Several works on the MOW distribution have concluded that the complex orography found in this region affects the MOW flow across this area. The exit of MOW from the Gulf of Cadiz is strongly affected by the existence of a narrow passage between Gorringe Bank and Cape St. Vincent (Figure 1). Zenk and Armi (1990) proposed a schematic flow pattern for the MOW after its passage through the "gateway" between Cape St. Vincent and the Gorringe Bank. Later studies have concluded

5 that, despite of most of the MOW flowing out of the Gulf of Cadiz turns northward through this narrow passage (Deniault et al., 1994), a second branch of the flow is deflected westward along the southern flank of the Gorringe Bank (Iorga and Lozier, 1999a and 199b).

Another feature commonly described in works on the distribution of MOW in the area is the formation of two gyres: The first one, a cyclonic gyre, attached to the Gulf of Cadiz centred at ~35ºN and ~9ºW with a diameter of ~250 Km (Iorga and Lozier,

10 1999a, and 1999b). The second one, is an anticyclonic gyre centred in the Tagus Basin, it is the main responsible of the accumulation area known as MOW reservoir (Iorga and lozier, 1999a and 1999b). It is worth to mention that the definition of the MOW reservoir has been widely used in several studies, however the geographic window used to define this area may differ considerably from the more restrictive definitions (e.g. Iorga and Lozier, 1999a; and Pascual et al. 2018) to the more relaxed ones (e.g. Potter and Lozier, 2004; Bozec, 2011).

15 The area covered by the Tagus anticyclonic gyre is a key location where the MOW is distributed on its two main advective pathways. North of the Tagus gyre, part of the flow diverges continuing northward beyond the Extremadura Promontory. The south boundary of the Tagus gyre is linked with the westward MOW branch defined by Reid (1994), the westward MOW branch is originated in the southern flank of Gorringe Bank, and it is feed by the split of the flow leaving the Gulf of Cadiz. This flow travels westward along the north wall of Horseshoe Basin (Iorga and Lozier, 1999a) and converges with a southward

20 geostrophic flow coming from the Tagus gyre (Iorga 1999a, Deniault et al., 1994). The formation of the so-called westward pathway is clear once the flow detaches of the mountain chain and penetrates westward into the North Atlantic. However, Iorga and Lozier (1999a and 1999b), using 80 years of hydrographic data and a diagnostic model, found that this branch does not suppose a significant westward advection of MOW into the subtropical gyre.

The general scientific consensus on the spread of MOW south of Gulf of Cadiz points out that it is largely supported by the

25 development of meddies originated southwest of the MOW reservoir and near the African continental slope (Zenk et al., 1992; Sangrá et al., 2009). The studies of the penetration of westward branch into the North Atlantic does not show a clear advective transport of MOW into the subtropical gyre, the formation of meddies is considered the main cause of the observed large-scale westward penetration of Mediterranean salt (Arham and King, 1995).

Some evidences suggest that there is some advective southward flow along the African continental slope. This flow is

30 originated in the cyclonic gyre centred in the Gulf of Cadiz (Iorga and Lozier, 1999a) and spreads southward being observed in latitudes of 32ºN (Machín and Pelegrí, 2009). The south boundary of the MOW is affected by the interaction with the overlying AAIW, thereby the salinity signal of MOW gets deeper in these latitudes (~1200m) due to the presence of the AAIW centred at about 800 m depth. According to Machin and Pelegrí (2009) the northern limit of AAIW is located around 32ºN near the African continental slope, however the presence of AAIW northward to the Canary Islands is subject to a seasonal

variability. The mixing processes between both water masses has been studied by van Aken (2000) concluding that the core of Antarctic Intermediate Water appears to contribute to the formation of MOW since it becomes entrained into the overflow near Gibraltar. This entrainment gives rise to an enhanced concentration of the nutrients in the Mediterranean water in the North Atlantic.

5   Several works have focused their interest in the temporal variability of MOW, they concluded that its variability comprises a wide range of time scales. Prieto et al. (2013) analysed a dataset of semiannual hydrographic stations located in the Iberian platform. Their findings point to, despite of interannual variability is larger, the seasonal signature represents a 20% of the overall interannual variability. This variability has been found along the continental slopes affected by MOW, it is a consequence of the variability of the slope current responsible of the northward transport of MOW along the European

10   continental slopes. In summertime the narrow jet is trapped at the continental slope, reinforces its thermohaline signature near the slope and diminishes thereby its presence at the outer ocean. In wintertime the slope flow weakens and even can be reversed in some areas (Fricourt et al., 2007; Prieto et al., 2013; Pascual et al., 2018).

Variability in longer time scales has been described in several studies, Potter and Lozier (2004) analysed 40 years of hydrographic data to calculate temperature and salinity trends of MOW reservoir. During this period, they found positive

15   temperature and salinity trends that leads to a heat content gain that overpasses the average gain of the North Atlantic basin over the latter half of the 20th century. Leadbetter et al. (2007) using three repeat sections at 36ºN in the North Atlantic, found an increase of MOW salinity from 1959 to 1981 followed by an almost compensating decrease in salinity from 1981 until 2005 in the upper-intermediate layers. According to their results, this change is controlled by water mass changes along neutral density surfaces suggesting a change in the source waters. Bozec et al. (2011) hypothesized that MOW water mass distribution

20   may be altered by changes in the circulation of the North Atlantic, to investigate this possible source of variability they used a set of model runs forced by either a climatological forcing or an interannual atmospheric forcing. They found a connection between salinity anomalies along the northern and the westward pathways, thereby they concluded that the observed salinity changes in the MOW reservoir can be explained by circulation-induced shifts in the salinity field in eastern North Atlantic basin.

25   **3 Data and methods**

The present study uses the IBI ocean reanalysis delivered by CMEMS (Levier et al., 2014; Sotillo et al. 2015; Aznar et al., 2016, Amo Baladrón, 2018). The domain covered by the IBI reanalysis is limited by the 26ºN and 56ºN parallels, and the 19ºW and 5ºE meridians and it provides daily averages of zonal and meridional velocity components for a period that ranges from January 1992 to December 2016, with a 1/12º horizontal resolution, and 75 vertical levels.

30   The numerical core of the IBI reanalysis is version 3.6 of eddy-permitting NEMO (Madec, 2008) ocean general circulation model. This model solves the three-dimensional finite-difference primitive equations in spherical coordinates discretized on an Arakawa-C grid. It assumes hydrostatic equilibrium and Bousinesq approximation. Vertical mixing is parameterized

according to a k-ε model implemented in the generic form proposed by Umlauf and Burchard (2003) including surface wave breaking induced mixing. The bathymetry is derived from GEBCO 08 dataset (Becker et al., 2009), merged with several local databases.

The IBI run is forced with atmospheric fields from the ECMWF ERA Interim (Dee et al., 2011). 10-m wind, surface pressure (added with inverse barometer approximation), 2-m temperature and relative humidity are provided at 3-hour frequency. On the contrary, precipitation and radiative fluxes are provided in daily averages from a modified ERA-interim reanalysis (Sotillo et al., 2015). CORE empirical bulk formulae (Large and Yeager, 2004) is used to compute latent sensible heat fluxes, evaporation and surface stress.

The IBI reanalysis use lateral open boundary data from the CMEMS global reanalysis (temperature, salinity, velocities and sea level) at 0.25° of resolution (Garric and Parent, 2018). These are complemented by eleven tidal harmonics built from FES2004 (Lyard et al., 2006) and TPXO7.1 (Egbert and Erofeeva, 2002). Fresh water river discharge are implemented as lateral open boundary condition for 33 rivers from observational and climatological data, additionally an extra coastal runoff rate climatology is used to make the IBI forcing consistent with the ones imposed in the global system (Maraldi et al. 2013).

The data assimilation scheme applied is the MERCATOR Ocean SAM2 (Lellouche et al., 2013), established from a Singular Extended Evolutive Kalman filter. Measurements from CMEMS CORA product (Cabanes et al., 2013; Gatti and Pouliquen, 2017) database are assimilated as well as high resolution Sea Surface Temperature data obtained from analysis of multi-satellite and AVHRR products, and remote sensing Sea Level Anomalies (SLA) measured by radar altimeter (Jason-3, Sentinel-3A, HY-2A, Saral/AltiKa, Cryosat-2, Jason-2, Jason-1, T/P, ENVISAT, GFO, ERS1/2).

This study is based in the regional analysis of the IBI averaged circulation at 1000m for the period 1992-2016. IBI reanalysis provides ocean fields at 947 and 1045 m depth, therefore in this work the 1000m depth fields shown are derived from the average of this two IBI levels. The results provide an average circulation field that offers information about the main transports occurring in the region. Since the time average is computed from daily data at 1/12° resolution, the analysed fields include the net mesoscale transports filtering its intrinsic temporal variability. The interannual variability of MOW and its associated oceanic patterns is studied by the analysis of the high/low salinity events in Horseshoe Basin at 1000m depth, these events are defined as the 10th and 90th percentiles of the salinity time series. The composites of temperature and salinity are derived from these events providing an image of the average ocean state under these conditions.

Part of the analysis performed is focused over three specific areas (boxes defined in Figure 1), these three regional domains have been selected taking in to account general circulation patterns. The analysis of water properties, circulation, and transports is made on average over each box, as well as on the sections limiting the boxes. The Horseshoe basin is split in two different boxes: The northern one (Gorringe Bank Box, GBB) comprises Gorringe Bank and the mountain chain to the west of it, the southern box (Ampere Bank Box, ABB) surrounds the Ampere Bank and the seamounts that conforms the southern boundary of Horseshoe Basin. The third box is defined north of the Canary Islands near to Cape Ghir (Cape Ghir Box, CGB), its limits

were established surrounding the bathymetric promontory located in the African continental slope between Cape Ghir and Cape Sim.

4 MOW regional circulation patterns

4.1 Tagus and Horseshoe Basins

5 Figure 2 shows the mean 1000m velocity field derived from IBI Reanalysis, MOW transport along the north slope of Gulf of Cadiz is a narrow stream that flows westward attached to the slope, average speeds in this region can reach 0.5-1 m s-1, this result is consistent with the current speeds found in literature (Gasser et al., 2017; Sánchez-Leal et al., 2017). South of the outflow stream, results suggest an eastward countercurrent that provides the required external water input to feed the intense entrainment processes suffered by MOW in the region (Ambar and Howe, 1979; Ochoa and Bray, 1991; Baringer and Price,

10 1997 ; Jia, 2000).

Beyond the Cape St. Vincent the flow is strongly affected by the orography. After the MOW moves out from the Gulf of Cadiz, the main stream is split by the presence of Gorringe Bank, one part of the flow turns northward through the narrow passage between Cape St-Vincent and Gorringe Bank and the other part continues westward south of this promontory. The northward path develops an intense stream that follows the Portuguese continental slope and enters into the Tagus Basin. After the flow

15 crosses the gateway, it diverges again to form two separated circulation areas: the bathymetric channelling of water towards the Tagus Basin leads to the formation of the widely-described Tagus Anticyclonic Gyre; and a narrow northward flow that, despite of the orographic elevations, goes northward following the margin defined by the continental slope.

The area comprised by the Tagus Basin and Gorringe Bank can be understood as the centre where the MOW is distributed in the North Atlantic. The narrow passage between Gorringe Bank and Cape St. Vincent forces the splitting of the flow exiting

20 the Gulf of Cadiz and promotes the formation of the two main advective pathways of MOW. The westward MOW pathway begins when the water masses detaches from the continental slope south and north of Gorringe Bank and travels following the chain of seamounts west of this promontory. In the south flank of the mountain range, the flow is forced by the limited transport through the Gorringe gateway; in the northern flank of the Gorringe Bank, the westward flow is promoted by the southern limit of the Tagus Anticyclonic Gyre. On the other hand, the northward MOW pathway commences after the MOW enters the

25 Tagus Basin, there the flow spits again to form two separated features: the Tagus Anticyclonic Gyre, and the poleward slope current which starts near a promontory in the Portuguese slope (37.8°N, 9.4°W) and travels northward up to the Extremadura Promontory. There, the northward flow converges with the northern closure of Tagus Anticyclonic Gyre and continues northward forming the poleward slope current that will follow the European continental slope up to Porcupine Bank.

Circulation in Horseshoe Basin is mainly characterized by two opposite zonal currents. The northern half of the basin shows

30 the westward current originated in Gorringe Bank, confirming the results suggested by Iorga and Lozier (1999a); this flow turns cyclonically once it reaches the west margin of the basin. In the southern half of the basin, the turning flow is channelized eastward influenced by the mountain chain of Ampere Bank. According to our results this flow continues eastward exiting the

Horseshoe Basin and returning back to the Gulf of Cadiz where, it provides the water masses requested to entrain by the Mediterranean Water Mases cascading in the Gulf of Cadiz slopes.

The analysis of the mean vorticity at 1000m (Figure 3) provides information about the main gyres occurring in the area. It is worth to mention that this field is affected by the shear of the flow near the continental slopes. This is the case of the noisy

5   values detected near the continental margins. The strong shear between the descending MOW flow and the surrounding water mases in the Northern slopes of Gulf of Cadiz leads to an area with the highest cyclonic vorticity in the figure, this vorticity values denotes the intense mixing processes taking place in the area. The bathymetry also has an important influence in all the sea mountains included in the domain, they are associated to high negative values of vorticity indicating anticyclonic circulation around them, even when the top of the obstacle is hundreds of meters below the level of 1000m depth, as it is the

10   case of the sea mount at 36.4ºN and 13.0ºW, whose summit is at 1893m depth. The Tagus Basin shows negative values of vorticity mainly related with the presence of the Tagus Anticyclonic Gyre. However, results in Horseshoe basin shows the presence of a generalized cyclonic circulation with two separated centres of vorticity located at 14ºW and 12ºW.

Regarding the cyclonic gyre near the Gulf of Cadiz suggested by previous studies (Iorga and Lozier, 1999a, and 1999b), the reanalysis does not provide a clear signal of positive vorticity centred around 35ºN and 9ºW. Results in this area show mainly

15   a zonal westward flow advecting water into the Gulf of Cadiz. In this area, the water transported eastward diverges taking two directions: part of the flow turns northward to be reincorporated into the main MOW current in the Iberian slopes, and a second part of the flow turns anticyclonically following the African slope towards the Seine Abissal Plain. The centre of this circulation is shown in the map of vorticity near the slope as an area of negative values at 34.2ºN and 9.2ºW. The splitting of the eastward flow entering the Gulf of Cadiz in two branches at 9.4ºW is favoured by the bathymetric zonal elevation at 35.3ºN in the Gulf

20   of Cadiz.

Volume transports have been computed in the limits of the two boxes defined around Gorringe Bank and Ampere Bank (GBB and ABB respectively). The analysis of transports though the limits of these boxes provide information about the water masses entering/leaving the Horseshoe Basin as well as the meridional transport thereof.

Figure 4 shows the mean velocities and net volume transport in the sections defined in GBB and ABB. Results show the main

25   input of MOW into the Horseshoe Basin is produced through the northern and eastern limits of GBB. The presence of Gorringe Bank highly influences the MOW flow coming from Cape St. Vincent. Part of this flow is deflected towards the Horseshoe Basin following the south flank of Gorringe Bank and enters the basin through the eastern-GBB limit. The input through the northern limit of GBB is induced by the seamounts at 36.2ºN and 14.5ºW which forces a southward transport of water from the Tagus Anticyclonic Gyre towards the Horseshoe Basin. The net transport in sections evidences that, despite of the

30   appreciable flow entering the basin through the eastern-GBB boundary (~0.7 Sv), the flow through the northern-GBB limit (~1.4 Sv) almost doubles it being the main source of MOW in Horseshoe Basin.

Attending to the water outputs in GBB, Figure 4 shows the presence of a westward transport that overpasses the seamounts and leaves the box by crossing the western boundary. This transport of about 1 Sv is the starting of the MOW westward

pathway described in bibliography (Iorga and Lozier, 1999a and 1999b). The latitudes where this westward flow can be appreciated ranges from 35.6ºN up to 37.2ºN.

The net meridional transport between the GBB and ABB is shown in Figure 4. The southward transport of water (~1 Sv) in Horseshoe Basin is mainly induced by the cyclonic turning of the westward current previously described in the basin, in

5 agreement with the results obtained by Iorga and Lozier (1999a, and 199b) the southward penetration of this water is stopped by the southern wall of the basin redirecting this flow eastward. However, results suggest a net external water input (~0.8 Sv) entering the basin through the southern boundary of ABB, the two converging flows are then redirected eastward exiting ABB towards the Gulf of Cadiz (~1.9 Sv). The θ/S diagrams averaged in GBB and ABB (Figure 3b) show the differences in temperature and salinity between the northern and southern half of Horseshoe Basin. Such differences mainly affect to the

10 upper-intermediate layers of ABB where a freshening and cooling of waters is appreciable. The water flow averaged in GBB presents the usual θ/S profile of MOW with a peak in salinity around 1000m depth (Leadbetter, 2007). On the contrary, the θ/S profile averaged in ABB shows the interaction of MOW with AAIW and North Atlantic Deep Water (NADW). The salinity peak is still found at approximately 1000m depth, however the influence of AAIW is evidenced by the temperature and salinity reduction in layers above the salinity peak (from 600 to 1000m depth) producing a concavity that sharpens the peak, the

15 influence of NADW is reflected in the freshening and cooling in deeper layers.

Despite of the net southward transport between GBB and ABB boxes, the averaged velocities between them reveals northward flows advecting water from ABB to GBB; this implies the existence of meridional mixing processes in Horseshoe Basin. The northward transport of modified water can be appreciated in the velocity and vorticity fields shown in Figures 2 and 3, the general circulation in Horseshoe Basin is composed by two separated centres of cyclonic vorticity, they are located at 35.7ºN

20 and 14.2ºW and at 35.7ºN and 12.0ºW. The circulation around these two centres promotes the north-South mixing in Horseshoes Basin. The θ/S profile averaged in the Eastern boundary of ABB evidences that the properties of water exiting the basin towards the Gulf of Cadiz are the result of the mixing between the southern and northern waters in Horseshoe Basin, however the mixing processes mainly affects the upper-intermediate layers above 1100m depth.

4.2 Cape Ghir

25 The average circulation pattern at 1000m shown in Figure 2 reveals the existence of a zonal current at 31.5ºN. It is formed in the African continental slope and conforms an advective westward flow that penetrates into the North Atlantic up to 16.2ºW. This current is associated with an area of cyclonic vorticity to the west of Cape Ghir centred at 30.5ºN and 11.6ºW (Figure 3). The domain CGB, near the Cape Ghir, has been defined to analyse the source of this flow (Figure 1). Figure 5 displays the velocity and water transport in the boundaries of CGB, it reveals the entrance of water masses from north as a weak southward

30 transport (~0.6 Sv) between 12ºW and 11ºW, and from south as a more intense transport (~3.0 Sv) close to the continental slope. The exit of water masses occurs crossing the western limit of CGB where a westward current of 5-8 cm/s (~3.2 Sv) pushes the converging water masses towards the outer ocean (Figure 5a). The θ/S diagram averaged in the limits of the domain shows the presence of the salinity peak at 1000m associated to the MOW (Figure 4b), however its temperature and salinity

values are significantly lower than values seen 500 km to the north at Horseshoe where the MOW salinity peak ranges between 35.9-36.0 PSU and 10.1-10.4 ºC. The water layers above the salinity peak reveals the strong influence of the AAIW by the presence of a concavity in the profile associated to the cooler and fresher AAIW. The result found in the Northern section of CGB is consistent with the observed climatological T/S diagram averaged from 10º to 12ºW and from 31º to 33ºN by Machín

5   and Pelegrí (2009). Comparing the θ/S profiles of the Northern and Southern boundaries of the GCB, results show a different relative contribution of MOW and AAIW in each section. While in the Southern-GCB boundary the θ/S profile shows a dominance of AAIW with reduced values of salinity and a concavity in the upper-intermediate waters; at the Northern-GCB section the θ/S diagram shows a greater influence of MOW with a sharper peak of salinity at 1000m. Attending to the θ/S diagram averaged in the Western boundary of the box, the outgoing waters reveals a profile influenced by the water masses

10   seen in the Northern and Southern boundaries of GCB. The peak of salinity diminishes and the values of temperature and salinity in the upper-intermediate layers are increases reducing its concavity. The analysis of the mean velocities shown in Figure 2 provides more information about the circulation processes taking place in this area. South of Cape Ghir the poleward slope flow mainly composed by AAIW follows the continental slope up to the promontory near Cape Ghir and even further (Machín and Pelegrí, 2009). There, the promontory and the opposition of the southward flow of MOW forces the cyclonic

15   turning of AAIW that detaches from the continental slope and starts an advective westward flow penetrating up to 16.2ºW. The intense mixing processes occurring on this confrontation leads to the mixing of MOW and AAIW.

5 Interannual variability

To analyse the interannual variability of MOW in the Horseshoe Basin, the anomalies of salinity at 1000m have been computed and averaged in the area composed by GBB and ABB. The analysis of the time series of salinity anomalies reveals a differential

20   behaviour of the maximum and minimum anomalies (Figure 6). While the maximum values of salinity are spread over the time, the minimum anomalies are comprised in a unique event occurring in the period 2000-2003. This low salinity event in the area is clear since all values under the 10th percentile of the time series are found in this period. This event is consistent with the results found by Bozec et al. (2011), who report a slight retreat of the inner salinity contours towards the east, especially after 2000.

25   The dates of the minimum and maximum anomalies of salinity defined as the values under/over the 10th/90th percentiles respectively have been used to derive the composites of the both the θ/S diagram averaged in the Horseshoe Basin (Figure 6b) and the meridional section of salinity at 36ºN coinciding with the limit between GBB and ABB (Figure7). Since each composite is derived from the fields averaged in the dates where the anomaly at 1000m depth is remarkably high or low, they represent the ocean state associated to these particular salinity conditions. Moreover, due to every minimum value selected is comprised

30   in the period 2000-2003, the derived minimum composite reflects mainly the ocean state under this specific low salinity event. The θ/S composites shown in Figure 6 reveal that variability in the Horseshoe Basin affects mainly the layers below the salinity peak. Under conditions of the minimum salinity event, the water masses below 1000m depth suffers a decrease of 0.25-0.75

PSU. Temperature is also affected, existing during this event a cooling of about ~0.6ºC. The structure of the water column is also modified, being the salinity peak associated to the MOW core pushed from the usual 1000m up to 800m depth.

Based on three repeat sections at 36ºN, Leadbeter et al. (2007) observed interannual variability of intermediate water masses between 10ºW and 20ºW. This variability mainly affected the layers above the salinity peak, whereas variability in lower levels were smaller. However, our results, based on the use of a high resolution regional reanalysis, suggest an inconsistency since the θ/S variability in this area mainly affects the layers below the MOW salinity peak. As presented in previous sections, variability above the salinity peak can be better attributed to latitudinal variations, the differences between θ/S diagrams averaged at GBB and in ABB (~100 Km southward) are mainly found in levels above the MOW salinity peak. On the contrary, according to the present analysis, the main temporal variability in the Horseshoe Basin is found in layers below the MOW tongue. The composite sections of salinity at 36ºN shown in Figure 7 depict the vertical structure of the water column under conditions of maximum and minimum salinity anomaly. Under conditions of the minimum salinity event (Figure 7a), results suggest a westward advance of the underlying NADW that leads to retreat of the MOW tongue together with an upward pushing of it. This process also implies a general freshening and cooling of the whole water column. The accumulation of low-salinity waters west of 15ºW and depths below 1100m, supports this hypothesis and suggests that penetration of the NADW into the Horseshoe basin is limited by the Azores-Portugal Rise. The perturbation in isohalines can be appreciated up to 400m above the top of the seamount. This result agrees with Bozec et al. (2011) who reported a similar behaviour of the boundary between MOW and the underlying LSW in the central Atlantic.

6 Conclusions

In the present work, an analysis of the spreading processes of MOW in the east North Atlantic has been performed though the use of a high resolution ocean reanalysis: the CMEMS IBI regional reanalysis. The ocean properties and flows are analysed at intermediate depths (500-2000m depth) in the Tagus, Horseshoe and Seine basins. These basins are adjacent to the Gulf of Cadiz and they conform the main area where the MOW is accumulated and spread into the North Atlantic. In this work we analyse the tongue of MOW in the reservoir area, the influence of bathymetry over the spreading of MOW, and its interactions with the surrounding water masses (NADW and AAIW). This work has been conducted, comparing also the IBI reanalysis with previous works on the characterization of MOW in the North Atlantic. The high agreement of results with the known features of MOW suggest a proper reproduction of the dynamic features of the intermediate waters in the region. Moreover, the high resolution of the IBI reanalysis product allows to describe new mesoscale features, not previously reported in literature.

One of the main contributions of this work results from the updated description of circulation patterns of MOW in the east North Atlantic. A coarse description of the circulation patterns in this area was reported by previous studies (Daniault et al., 1994; Mazé et al, 1997; Iorga and Lozier, 1999a; 1999b; van Aken, 2000), however the high resolution of IBI reanalysis allows a more detailed description of the circulation in the region. In Figure 8, it has been summarized the circulation patterns

described by the abovementioned works (black arrows) and the updated scheme, resulting from the IBI reanalysis data (represented by red arrows). Once the recently formed MOW overpasses Cape St. Vincent, the presence of Gorringe Bank splits the flow in two branches: one of them enters the Tagus Basin, describing an anticyclonic gyre, whereas the other branch of MOW flows westward along the northern boundary of the Horseshoe Basin. The bathymetry also forces the cyclonic

5   circulation in Horseshoe Basin, the westward flow started in Gorringe Bank turns cyclonically when it encounters the seamounts in the western boundary of the basin (the Azores-Portugal Rise). Thereafter, water masses recirculates eastward towards the Gulf of Cadiz. Seamounts of the Ampere mountain chain lead to the formation of anticyclonic vorticity in the proximity of these obstacles, and circulation around these centres favour active transports of southern water into Horseshoes Basin. The external water entrained is mainly composed by a diluted form of AAIW in the upper-intermediate layers and

10   NADW in depths below 1000m. Thereby, the MOW water masses that recirculates into the Gulf of Cadiz are previously modified in Horseshoe by mixing with AAIW and NADW. This process could explain the presence of an enhanced concentration of nutrients in the MOW, as reported by Van Aken (2000).

The interaction between MOW and the deeper AAIW near the African continental slope is highly influenced by the bathymetric promontory between Cape Ghir and Cape Sim. The converging flows of MOW, which travels southward along the African

15   Continental slope; and the northward transport of AAIW, that enters the basin through a narrow gateway between Fuerteventuran and the African Shelf, collides in this area producing a zonal transport of mixed MOW-AAIW waters towards the inner ocean. The potential role of this branch as advective pathway for MOW into the subtropical gyre and its relationships with the Madeira Eddy Corridor, described by Sangrá et al. (2009), will be analyzed in future works.

The analysis of the circulation patterns in the region has highlighted the role of bathymetry as a key factor determining the

20   spreading and mixing patterns of MOW in the region. The presence of three abyssal plains separated by seamount chains implies an orographic complexity that highly influences these processes in the area. This work has also reported some cases where the bathymetric features can modify the flow hundreds of meters above the obstacle, moreover the coinciding topographic features with the preferred areas of meddy formation described by previous authors (Sangrá et al, 2009) suggest some influence of bathymetric obstacles favouring the meddy formation. Therefore, in other to obtain a realistic representation

25   of the ocean, the influence of the high resolution bathymetry must be considered by modelling studies in this region and depths. The analysis of the CMEMS IBI currents and transports together with the hidrographyc patterns derived has allowed the reconstruction of the dynamic variability in Horseshoe Basin. The composite analysis of temperature and salinity in the region leads to the conclusion of the main source of interannual variability in Horseshoe commes from the deeper layers of MOW. Our work has shown that the boundary between the MOW and the underlying NADW is subject to interannual variability.

30   According to the limited length of the CMEMS IBI reanalysis (25 years), the presence of the MOW tongue in Horseshoe Basin seems to be the normal situation. However, the reanalysis reveals the existence of a remarkable event (2000-2004) where the NADW advances into Horseshoe Basin. Under these specific conditions, the MOW core retreats eastward, diminishing the salinity in the whole water column.

Ocean Science
Discussions

Open Access

EGU

References

Ambar, I., Howe, M. R.: Observations of the Mediterranean outflow. II. The deep circulation in the vicinity of the Gulf of Cadiz. Deep-Sea Res., 26A, 555–568, 1979.

5   Amo Baladrón, A., Levier, B., Sotillo, M. G.: Product User Manual for Atlantic-Iberian Biscay Irish-Ocean Physics Reanalysis Product: IBI_REANALYSIS_PHYS_ 005_002, Copernicus Marine Environment Monitoring Service, http://cmems-resources.cls.fr/documents/PUM/CMEMS-IBI-PUM-005-002.pdf, 2018.

Arhan, M., King, B., Lateral mixing of the Mediterranean water in the eastern North Atlantic, Journal of Marine Research, 53,
10 6,865-895, doi:10.1357/0022240953212990, 1995.

Armi, L., Hebert, D., Oakey, N., Price, J., Richardson, P., Rossby, H., Ruddinck, B.: Two years in the life of a Mediter- ranean salt lens. J. Phys. Oceanogr., 19, 354–383, 1989.

15 Armi, L., Zenk, W.: Large lenses of highly saline Mediterranean water. Journal of Physical Oceanography, 14, 1560-1576, 1984.

Aznar, R., Sotillo, M. G., Cailleau, S., Lorente, P., Levier, B., Amo-Baladrón, A., Reffray, G., Álvarez-Fanjul, E.: Strengths and weaknesses of the CMEMS forecasted and reanalyzed solutions for the Iberia-Biscay-Ireland (IBI) waters, Journal of
20 Marine Systems, 159, 1-14, doi:10.1016/j.jmarsys.2016.02.007, 2016.

Baringer, M. O., Price, J. F.: Mixing and spreading of the Mediterranean outflow, J. Phys. Oceanogr., 27, 1654–1677, 1997.

Becker, J.J., Sandwell, D.T., Smith, W.H.F., Braud, J., Binder, B., Depner, J., Fabre, D., Factor, J., Ingalls, S., Kim, S.-H.,
25 Ladner, R., Marks, K., Nelson, S., Pharaoh, A., Trimmer, R., von Rosenberg, J., Wallace, G., Weatherall, P.: Global bathymetry and elevation data at 30 arc seconds resolution: SRTM30_PLUS. Mar. Geod., 32, 355–371, doi:10.1080/01490410903297766, 2016.

Bower, A. S., Lecann, B., Rossby, T., Zenk, W., Gould, J., Speer, K., Richardson, P. L., Prater, M. D., Zhang H.-M. Directly
30 measured mid-depth circulation in the northeastern North Atlantic Ocean, Nature, 419, 603–607, doi:10.1038/nature01078, 2002.

Bower, A., Armi, L., Ambar, I.: Lagrangian observations of meddy formation during A Mediterranean Undercurrent Seeding Experiment, J. Phys. Oceanogr., 27, 2545-2575, 1997.

Bozec, A., Lozier, M. S., Chasignet, E.P., Halliwel, G. R.: On the variability of the Mediterranean Outflow Water in the North
5   Atlantic from 1948 to 2006, J. of Geof. Res., 116, C09033, doi:10.1029/2011JC007191, 2011.

Cabanes, C., Grouazel, A., von Schuckmann, K., Hamon, M., Turpin, V., Coatanoan, C., Paris, F., Guinehut, S., Boone, C., Ferry, N., de Boyer Montegut, C., Carval, T., Reverdin, G., Pouliquen, S., Le Traon, P.-Y.: The CORA dataset: validation and diagnostics of in-situ ocean temperature and salinity measurements, Ocean Sci., 9, 1–18, doi:10.5194/os-9-1-2013, 2013.
10

Daniault, N., Mazé, J. P., Arhan, M.: Circulation and mixing of Mediterranean water west of the Iberian Peninsula, Deep Sea Research, 41, 11-12, doi: 10.1016/0967-0637(94)90068-X, 1994.

Dee, D. P., Uppala, S. M., Simmons, A. J., Berrisford, P., Poli, P., Kobayashi, S., Andrae, U., Balmaseda, M. A., Balsamo, G.,
15   Bauer, P., Bechtold, P., Beljaars, A. C. M., van de Berg, L., Bidlot, J. R., Bormann, N., Delsol, C., Dragani, R., Fuentes, M., Geer, A. J., Haimberger, L., Healy, S. B., Hersbach, H., Hólm, E. V., Isaksen, L., Kallberg, P., Köhler, M., Matricardi, M., McNally, A. P., Monge-Sanz, B. M., Morcrette, J. J., Park, B. K., Peubey, C., de Rosnay, P., Tavolato, C., Thépaut, J. N., Vitart, F.: The ERA-interim reanalysis: configuration and performance of the data assimilation system, Q. J. R. Meteorol. Soc., 137, 553–597, doi:10.1002/qj.828, 2016.
20

Egbert, G.D., Erofeeva, S.Y.: Efficient inverse modeling of Barotropic Ocean tides, J. Atmos. Ocean. Technol., 19, 183–204, doi:/10.1175/1520- 0426(2002)019b0183:EIMOBON2.0.CO;2, 2002.

Friocourt, Y., Levier, B., Speich, S., Blanke, B., Drijfhout, S. S.: A regional numerical ocean model of the circulation in the
25   Bay of Biscay, Journal of Geophysical Research: Oceans, 112, 9, 1-19, doi:10.1029/2006JC003935, 2007

García-Lafuente, J., Delgado, J., Criado-Aldeanueva, F., Bruno, M., del Río, J., Miguel Vargas, J.: Water mass circulation on the continental shelf of the Gulf of Cádiz, Deep-Sea Research Part II, 53, 11-13, 1182-1197, doi:10.1016/j.dsr2.2006.04.011, 2006.
30

Garric, G., Parent, L.: Product User Manual for Global Ocean Reanalysis Product: GLOBAL-REANALYSIS-PHY-001-025, Copernicus Marine Environment Monitoring Service, http://cmems-resources.cls.fr/documents/PUM/CMEMS-GLO-PUM-001-025.pdf, 2018.

Gasser, M. Pelegrí, J. L., Emelianov, M., Bruno, M., Grácia, E., Pastor, M., Peters, H., Rodríguez-Santana, A., Salvador, J., Sánchez-Leal, R. L.: Tracking the Mediterranean outflow in the Gulf of Cadiz, Progress in Oceanography, 157, 47-71, doi: 10.1016/j.pocean.2017.05.015, 2017.

Gasser, M., Pelegrí, J. L., Emelianov, M., Bruno, M., Gràcia, E., Pastor, M., Peters, H., Rodríguez-Santana, Á., Salvador, J., Sánchez-Leal, R. F.: Tracking the Mediterranean outflow in the Gulf of Cadiz, Progress in Oceanography, 157, June, 47-71, doi:10.1016/j.pocean.2017.05.015, 2017.

Gatti, J., Pouliquen, S.: Product user manual for near real time and delayed mode objective analysis products INSITU_GLO_TS_OA_REP_OBSERVATIONS_013_002_ab Period covered: 1990-2015, Copernicus Marine Environment Monitoring Service, http://cmems-resources.cls.fr/documents/PUM/CMEMS-INS-PUM-013-002-ab.pdf, 2017.

Iorga, M. C., Lozier, M. S.: Signatures of the Mediterranean outflow from a North Atlantic climatology 1. Salinity and density fields, J. of Geof. Res., 104, C11, 25985-2609, 1999a.

Iorga, M. C., Lozier, M. S.: Signatures of the Mediterranean outflow from a North Atlantic climatology 2. Diagnostic velocity fields, J. of Geof. Res., 104, C11, 26011-26029, 1999b.

Jia, Y.: Formation of an Azores Current Due to Mediterranean Overflow in a Modeling Study of the North Atlantic, Journal of Physical Oceanography, 30, 9, doi:10.1175/1520-0485(2000)030<2342:FOAACD>2.0.CO;2, 2000.

Large, W.G., Yeager, S.G.: Diurnal to Decadal Global Forcing for Ocean and Sea-Ice Models: the Data Sets and Flux Climatologies, NCAR technical note, NCAR/TN-460+STR, 2004.

Leadbetter, S. J., Williams, R. G., McDonagh, E. L., King, B. A.: A twenty year reversal in water mass trends in the subtropical North Atlantic, Geophysical Research Letters, 2007, 34, 12, 1-6, doi:10.1029/2007GL029957, 2007.

Lellouche, J.-M., Le Galloudec, O., Drévillon, M., Régnier, C., Greiner, E., Garric, G., Ferry, N., Desportes, C., Testut, C.-E., Bricaud, C., Bourdallé-Badie, R., Tranchant, B., Benkiran, M., Drillet, Y., Daudin, A., De Nicola, C.: Evaluation of global monitoring and forecasting systems at Mercator Océan, Ocean Sci., 9, 1, 57–81, doi:10.5194/os-9-57-2013 ,2013.

Levier, B., Benkiran, M., Reffray, G., Sotillo, M. G.: IBIRYS: A Regional High Resolution Reanalysis (Physical and Biogeochemical) over the European North East Shelf, EGU General Assembly, id.14014, 2014.

Lozier,M. S., Stewart N. M.: On the temporally varying penetration of Mediterranean overflow waters and eastward penetration of Labrador Sea Water, J. Phys. Oceanogr., 38, 2097–2103, doi:10.1175/2008JPO3908.1, 2008.

5   Lyard, F., Lefevre, F., Letellier, T., Francis, O.: Modelling the global ocean tides: modern insights from FES2004. Ocean Dyn., 56, 394–415, doi:10.1007/ s10236-006-0086-x, 2006.

Madec, G.: NEMO Ocean General Circulation Model, Reference Manual, Internal Report, LODYC/IPSL, Paris, 2008.

10   Machín, F., Pelegrí, J. L.: Northward Penetration of Antarctic Intermediate Water off Northwest Africa, Journal of Physical Oceanography, 39, 3, 512-535, 2009.

Machín, F., Pelegrí, J. L., Marrero-Díaz, A., Laiz, I., Ratsimandresy, A. W.: Near-surface circulation in the southern Gulf of Cádiz, Deep-Sea Research Part II, 53, 11-13, 1161-1181, doi: 10.1016/j.dsr2.2006.04.001, 2006.

15

Maraldi, C., Chanut, J., Levier, B., Reffray, G., Ayoub, N., De Mey, P., Lyard, F., Cailleau, S., Drévillon, M., Fanjul, E.A., Sotillo, M.G., Marsaleix, P., and the Mercator team: NEMO on the shelf: assessment of the Iberia-Biscay-Ireland configuration. Ocean Sci., 9, 745-771, doi:10.5194/os-9-745-2013, 2013.

20   Mazé, J. P., Arhan, M., Mercier, H.: Volume budget of the eastern boundary layer off the Iberian Peninsula, Deep-Sea Research Part I, 44, 9-10, 1543-1574, doi:10.1016/S0967-0637(97)00038-1, 1997

McCartney, M., Mauritzen, C.: On the origin of the warm inflow to the Nordic Seas, Prog. Oceanogr., 51, 125–214, doi:10.1016/S0079- 6611(01)00084-2. 2001.

25

New, A. L., Barnard, S., Herrmann, P., Molines J.-M.: On the origin and pathway of saline inflow to the Nordic Seas: Insights from the models, Prog. Oceanogr., 48, 255–287, doi:10.1016/S0079-6611(01) 00007-6, 2001.

Ochoa, J., Bray, N. A.: Water mass exchange in the Gulf of Cadiz. Deep-Sea Res., 38, S1, 5465–5503, 1991.

30

Pascual, Á., Levier, B., Sotillo, M.: Characterisation of Mediterranean outflow water in the Iberian-Gulf of Biscay-Ireland region, In: Copernicus Marine Service Ocean State Report, Issue 2, Journal of Operational Oceanography, 11, sup1, s1-s142, doi:10.1080/1755876X.2018.1489208, 2018.

Ocean Science
Discussions

Potter, R. A., Lozier, M. S.: On the warming and salinification of the Mediterranean outflow waters in the North Atlantic, Geophysical Research Letters, 31, 1, 1-4, doi:10.1029/2003GL018161, 2004.

Prieto, E., González-Pola, C., Lavín, A., Sánchez, R. F., Ruiz-Villarreal, M.: Seasonality of intermediate waters hydrography
5   west of the Iberian Peninsula from an 8 yr semiannual time series of an oceanographic section, Ocean Science, 9, 2, 411-429, doi:10.5194/os-9-411-2013, 2013.

Reid, J. L.: On the total geostrophic circulation of the North Atlantic Ocean: Flow patterns, tracers, and transports, Prog. Oceanogr., 33, 1–92, doi:10.1016/0079-6611(94)90014-0, 1994.
10
Reid, J. L.: On the contribution of the Mediterranean Sea outflow to the Norwegian-Greenland Sea, Deep Sea Res., Part A, 26, 1199–1223, doi:10.1016/0198-0149(79)90064-5, 1979.

Sánchez-Leal, R. F., Bellanco, M. J., Fernández-Salas, L. M., García-Lafuente, J., Gasser-Rubinat, M., González-Pola, C.,
15 Hernández-Molina, F. J., Pelegrí, J. L., Peliz, A., Relvas, P., Roque, D., Ruiz-Villarreal, M., Sammartino, S., Sánchez-Garrido, J. C.: The Mediterranean Overflow in the Gulf of Cadiz: A rugged journey, Science Advances, 3, 11, 1-12, doi:10.1126/sciadv.aao0609, 2017.

Sangrà, P., Pascual, A., Rodríguez-Santana, Á., Machín, F. Mason, E., McWilliams, J. C., Pelegrí, J. L., Dong, C., Rubio, A.,
20 Arístegui, J., Marrero-Díaz, Á., Hernández-Guerra, A., Martínez-Marrero, A., Auladell, M.: The Canary Eddy Corridor: A major pathway for long-lived eddies in the subtropical North Atlantic, Deep-Sea Research Part I, 56, 2100-2114, doi:10.1016/j.dsr.2009.08.008, 2009.

Sotillo, M. G., Cailleau, S., Lorente, P., Levier, B., Aznar, R., Reffray, G., Amo-Baladrón, A., Chanut, J., Benkiran, M.,
25 Álvarez Fanjul, E.: The MyOcean IBI Ocean forecast and reanalysis systems: operational products and roadmap to the future Copernicus Service, J. Oper. Oceanogr., 8, 1, 63–79, doi:10.1080/1755876X.2015.1014663, 2015.

Talley, L. D., McCartney, M. S.: Distribution and Circulation of Labrador Sea Water, Journal of Physical Oceanography, 12, 11, 1189-1205, doi:10.1175/1520-0485(1982)012<1189:DACOLS>2.0.CO;2, 1982.
30
Umlauf, L., Burchard, H.: A generic length-scale equation for geophysical turbulence models, J. Mar. Res., 61, 235–265, doi:10.1357/002224003322005087, 2003.

van Haken, H.: The hydrography of the mid-latitude Northeast Atlantic Ocean II: The intermediate water masses, Deep-Sea Research, 47, 5, 789-824, doi: 10.1016/S0967-0637(99)00112-0, 2000.

van Aken, H. M., Becker, G.: Hydrography and through-fow in the north-eastern North Atlantic Ocean: the NANSEN project. Progress in Oceanogaphy 38, 297-346, 1996.

von Schuckmann, K., Le Traon, P.-Y., Smith, N., Pascual, A., Braseur, P., Fennel, K., Djavidnia, S.: Copernicus Marine Service Ocean State Report, Issue 2, Journal of Operational Oceanography, 11, sup1, s1-s142, doi:10.1080/1755876X.2018.1489208, 2018.

von Schuckmann, K., Le Traon, P-T., Alvarez-Fanjul, E., Axell, L., Balmaseda, M., Breivik, L.-A., Brewin, Robert, J. W., Bricaud, C., Drevillon, M., Drillet, Y., Dubois, C., Embury, O., Etienne, H., Sotillo, M. G., Garric, G., Gasparin, F., Gutknecht, E., Guinehut, S., Hernandez, F., Juza, M., Karlson, B., Korres, G., Legeais, J.-F., Levier, B., Lien, V. S., Morrow, R., Notarstefano, G., Parent, L., Pascual, Á., Pérez-Gómez, B., Perruche, C., Pinardi, N., Pisano, A., Poulain, P.-M., Pujol, I. M., Raj, R. P., Raudsepp, U., Roquet, H., Samuelsen, A., Sathyendranath, S., She, J., Simoncelli, S., Solidoro, C., Tinker, J., Tintoré, J., Viktorsson, L., Ablain, M., Almroth-Rosell, E., Bonaduce, A., Clementi, E., Cossarini, G., Dagneaux, Q., Desportes, C., Dye, S., Fratianni, C., Good, S., Greiner, E., Gourrion, J., Hamon, M., Holt, J., Hyder, P., Kennedy, J., Manzano-Muñoz, F., Melet, A., Meyssignac, B., Mulet, S., Buongiorno Nardelli, B., O'Dea, E., Olason, E., Paulmier, A., Pérez-González, I., Reid, R., Racault, M.-F., Raitsos, D. E., Ramos, A., Sykes, P., Szekely, T., Verbrugge, N.: The Copernicus Marine Environment Monitoring Service Ocean State Report, Journal of Operational Oceanography, 9, sup2, s235-s320, doi:10.1080/1755876X.2016.1273446, 2016.

Warmer, R.: Towards a regional-ocean model for the behaviour of Mediterranean Outflow Water,

Zenk, W., Armi, L.: The complex spreading pattern of Mediterranean Water off the Portuguese continental slope, 37, 12, 1805-1823, doi: 10.1016/0198-0149(90)90079-B, 1990.

Zenk W., Schultz Tokos, K., Boebel, O.: New observations of meddy movement south of the Tejo Plateau. Geophysical Research Letters, 19, 2389-2392, 1992.
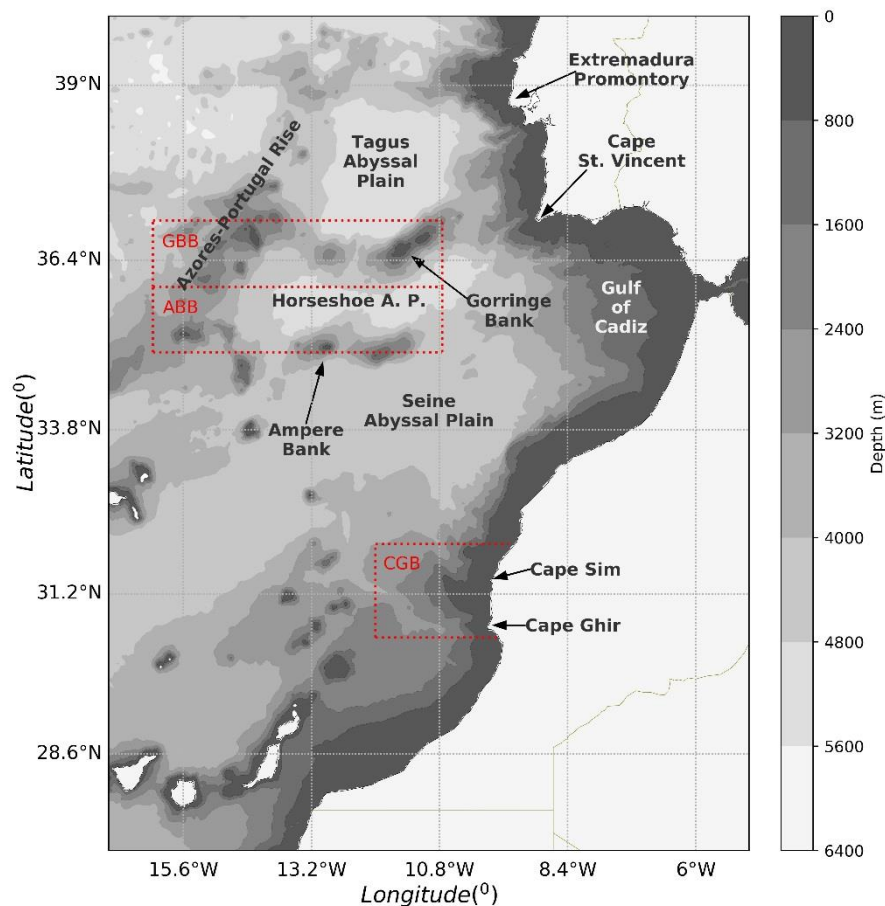
Figure 1: Map of the study domain showing geographical features mentioned in the text. Red dotted lines denote the sections where the transports have been computed. They define the three study boxes used in the present work: Gorringe Bank Box (GBB), Ampere Bank Box (ABB), and Cape Ghir Box (CGB).
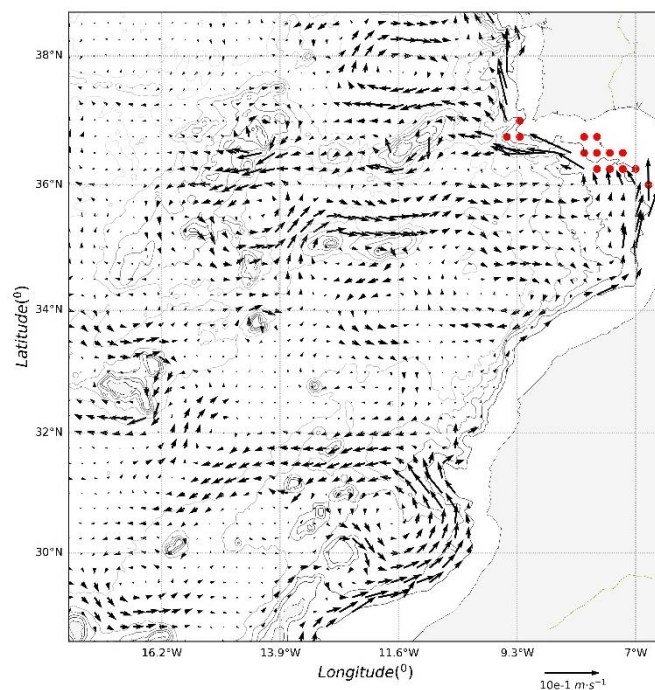
Figure 2: Velocity field at 1000m given by the CMEMS IBI reanalysis. For clarity reasons, grid points with very high relative velocities have been masked near the southern Iberian platform.
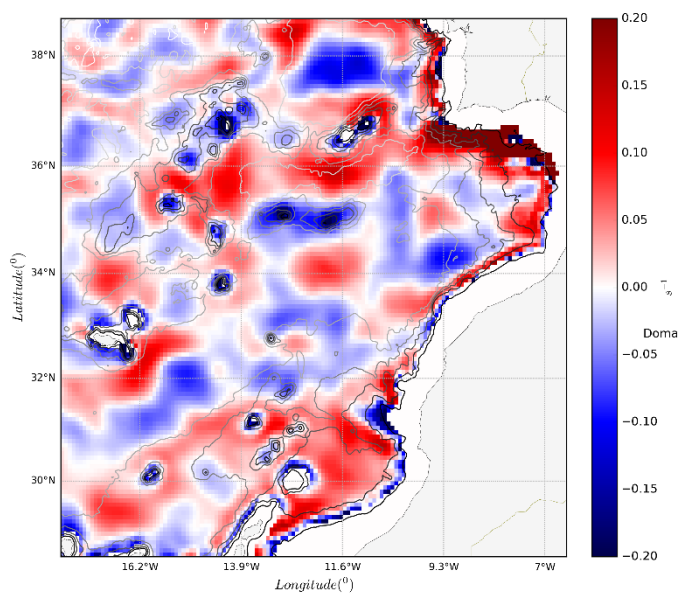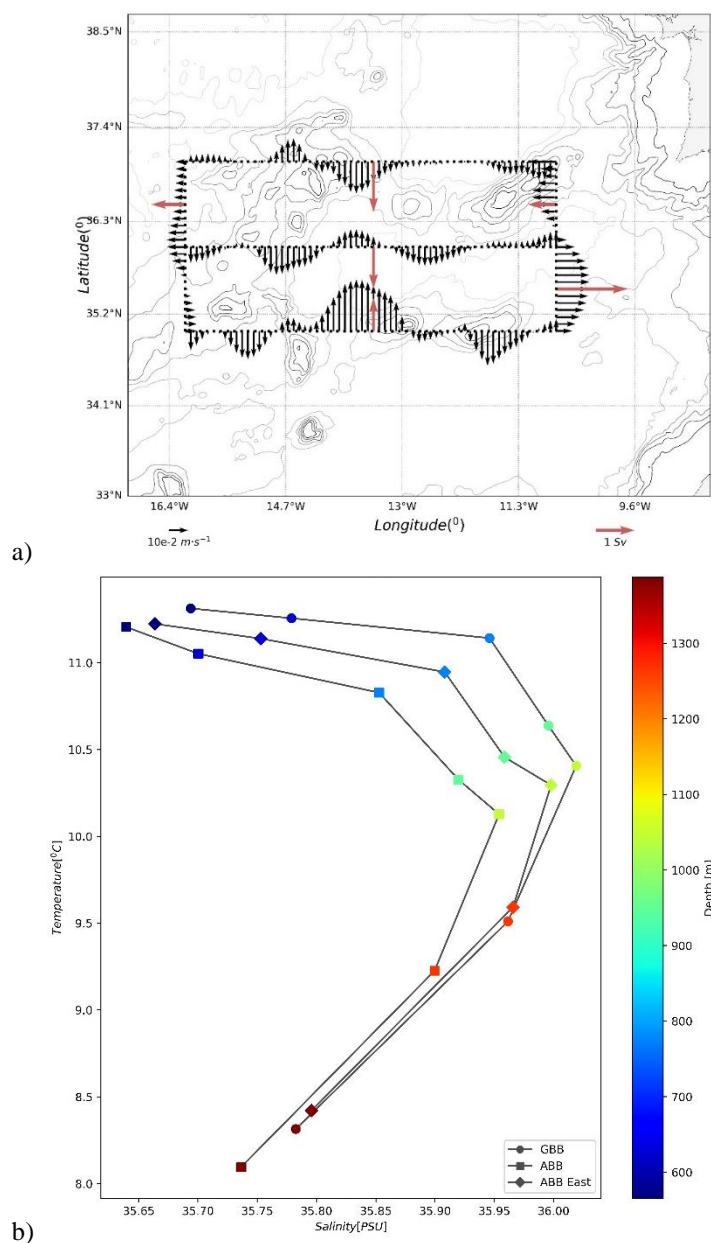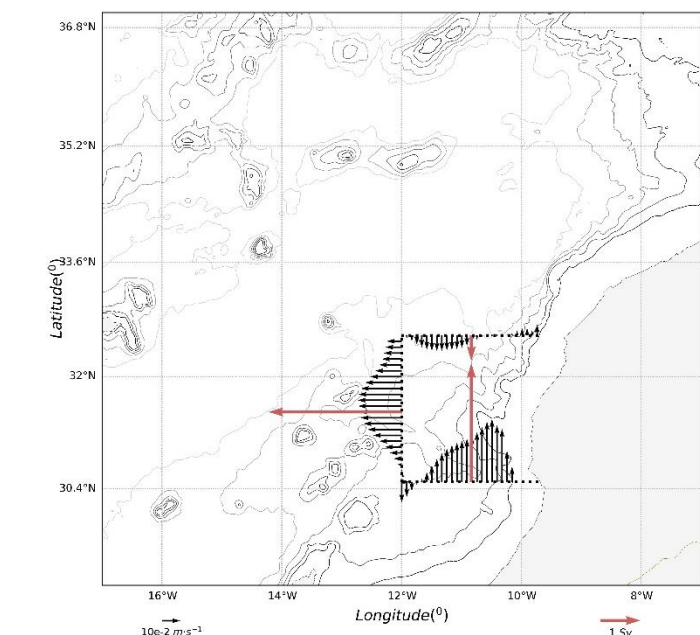
5

Figure 3: Vorticity field derived from IBI velocities. Red/blue colours denote cyclonic/anticyclonic vorticity, respectively.

a)

b)

Figure 4: (a) Transverse velocity (black arrows) and net volume transport (red arrows) in sections limiting GBB and ABB. (b) Mean θ/S diagram averaged in GBB (circles), ABB (squares) and along the section defining the Eastern-ABB boundary (diamonds).
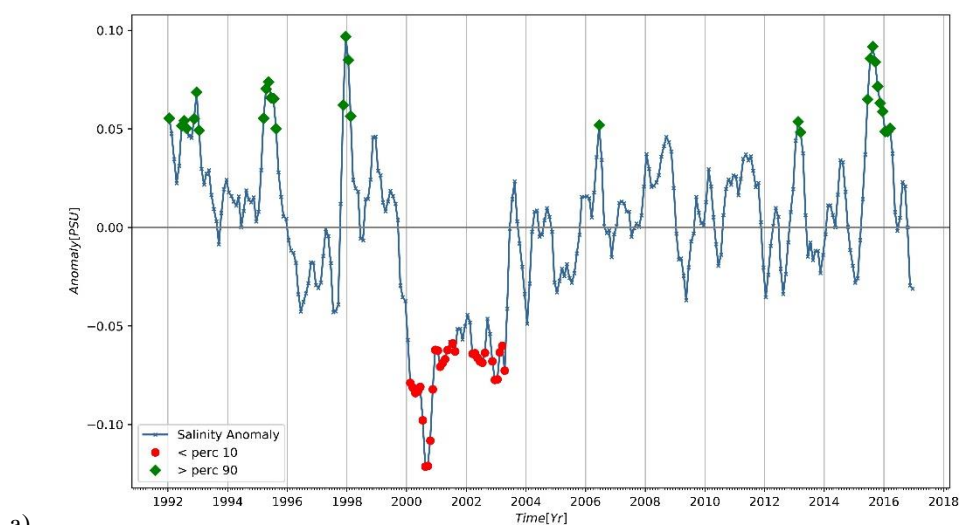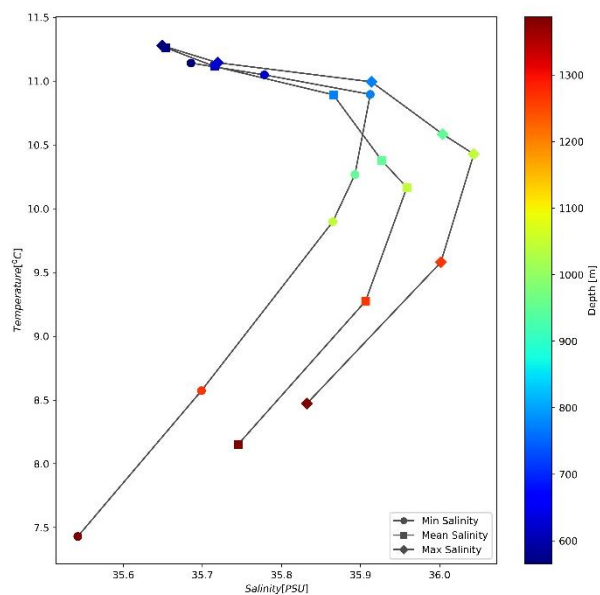
a)

b)

Figure 5: (a) Transverse velocity (black arrows) and net volume transport (red arrows) in sections limiting CGB. (c) Mean θ/S
5 **diagram averaged along the sections defining the Northern-CGB boundary (circles), Southern-CGB boundary (squares) and**
Eastern-CGB boundary (diamonds).

Ocean Science

Discussions

Open Access

a)

b)

Figure 6: (a) Anomalies of salinity at 1000m averaged in the whole Horseshoe Basin (areas GBB and ABB combined). Red/green dots depicts the values under/over the 10th/90th percentile of the time series. (b) θ/S diagram in Horseshoe Basin (areas GBB and ABB combined) averaged in the complete time record (squares), dates of minimum salinity (circles), and dates of maximum salinity (diamonds).
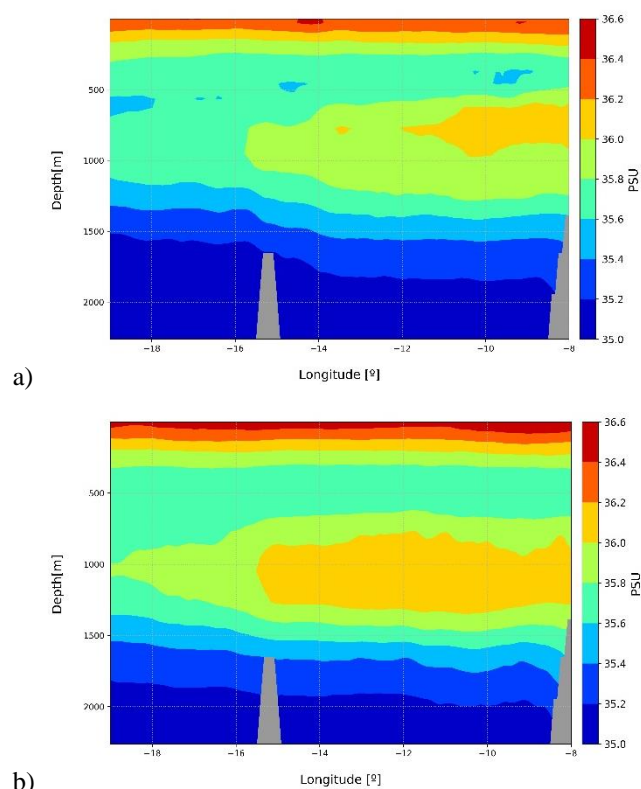
5

a)

b)

Figure 7: Composites of salinity at 36ºN (coinciding with the limit between GBB and ABB) averaging dates of minimum (a) and maximum (b) salinity defined by the 10th and 90th percentiles of salinity anomalies in Horseshoes Basin respectively.

5

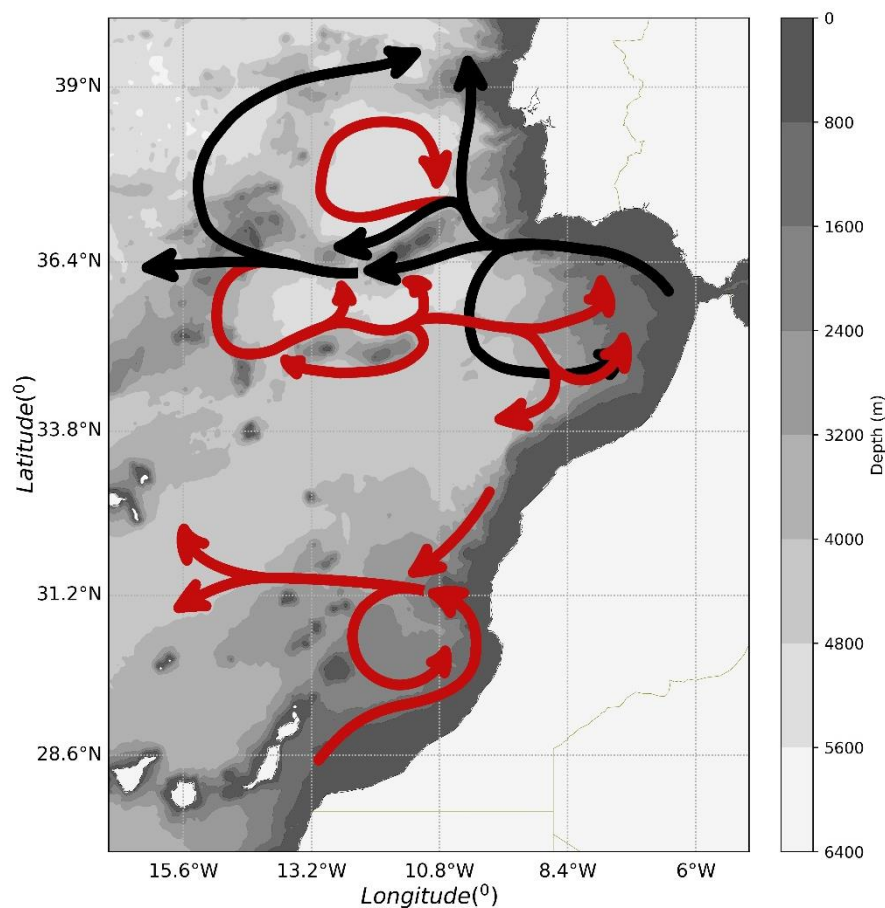Ocean Science
Discussions

Figure 8: Schematic representation of the overall Mediterranean Outflow Water pathways in the eastern North Atlantic. Black arrows show the current scientific consensus according to Iorga and Lozier (1999a). Red arrows summarize other MOW features described in the work. Results based on an analysis of the CMEMS IBI reanalysis (25 years record and 1/12° resolution).

5